New Techniques for In-situ Observations of Crack Growth Behaviour

T.J. Marrow

Materials Performance Centre, The University of Manchester, UK

james.marrow@manchester.ac.uk

Keywords: synchrotron computed tomography, diffraction contrast tomography, digital image correlation, stress corrosion, fracture, stainless steel, graphite.

Abstract

Experimental observations are essential for the validation for models for crack growth behaviour, particularly in the short crack regime. This paper reports the use of several new methods applied to in-situ short crack observation, including 3D observations of microstructure and cracking by synchrotron tomography techniques, and 2D optical digital image correlation. The examples presented include stress corrosion of stainless steels in aqueous environments, and brittle fracture of of nuclear graphite, where these new methods enable the visualisation of cracks in circumstances in which they would generally be regarded as practically non-observable.

Introduction

Short cracks may be defined as being either short relative to component or specimen dimensions, short relative to a characteristic microstructure length scale or physically short relative to engineering length scales (i.e. <1 mm). The lifetime of a component that suffers from fatigue or stress corrosion may be dominated by the period when the crack is short, particularly in terms of its physical size. The reliability of the prediction of component lifetime may therefore be very sensitive to the accuracy of models used to describe the short crack behaviour. It is well recognized that fracture mechanics descriptions for crack behaviour are length scale dependent, and there is a substantial literature to describe short fatigue crack behaviour (e.g [1]). In a similar manner, the brittle fracture of ceramic materials can also be strongly sensitive to the small defects [2]. The variability of strength in such materials may be described by the probability of occurrence of cracks within a certain strained region of material, and their conditions for instability [3]. The current understanding for these examples has been supported by direct observations of short crack behaviour, which have been used to construct and verify predictive models.

Short cracks can, by their very nature, be rather difficult to study. There are particular challenges for studies of crack nuclei in low toughness materials, where crack opening displacements are small and the use of high-resolution techniques may limit the size of the surveyed region. For environmentally assisted cracking, it can be also important for the sample to remain in the active environment throughout the observation. For example, the kinetics of crack development may be sensitive to the development of the crack tip chemistry, which may differ from the bulk environment [4].

This paper reports the use of several methods for in-situ short crack observations that enable the visualisation of cracks in circumstances in which they would generally be regarded as non-observable. The objective is to demonstrate how such quantitative observations can inform microstructure-based models of crack development. Several examples, using current research at the University of Manchester, are presented to illustrate the use of these techniques.

Synchrotron Computed Tomography

Computed tomography enables three-dimensional visualisation of the structure of materials [5]. Third generation light sources such as the European Synchrotron Radiation Facility (ESRF) allow rapid high-resolution (typically sub-micron), 3D computed tomography (CT) observations, quite suitable for in-situ experiments involving stress corrosion and fatigue in metals. The initiation, nucleation and growth of individual short fatigue cracks can therefore be studied in three-dimensions, in a manner analogous to 2D "replica" based techniques, [6][7][8]. Similar observations have also been reported for intergranular corrosion [9] and stress corrosion cracking [10]. A significant advantage of tomography experiments is the ability to interrogate the history of damage development, using datasets collected throughout the experiment.

For example, in an investigation of a sensitised austenitic stainless steel [10][11], observations were obtained for crack bridging by individual grain boundaries that are resistant to stress corrosion cracking (Figure 1); these non-sensitised, corrosion resistant grain boundaries failed in a ductile manner at high strain. They have been proposed to mechanically restrict the opening of the crack tip in a manner analogous to fibres in a composite material. Such crack bridging would reduce the in-elastic crack tip strains in response to the applied stress, and consequently decrease the stress corrosion crack growth rate. Three-dimensional modelling of intergranular stress corrosion crack nucleation, based on these observations, predicted that grain boundary engineering to increase the proportion of sensitisation resistant boundaries should significantly increase the incubation period for crack nuclei, and thereby increases intergranular SCC resistance [11][12]. Validation and further development of such IGSCC models, to address intergranular strains from grain misorientations [13] for example, requires observations of the interaction between cracks and microstructure. Ideally this should employ full three-dimensional characterisation of the microstructure itself. Diffraction Contrast Tomography can achieve this.

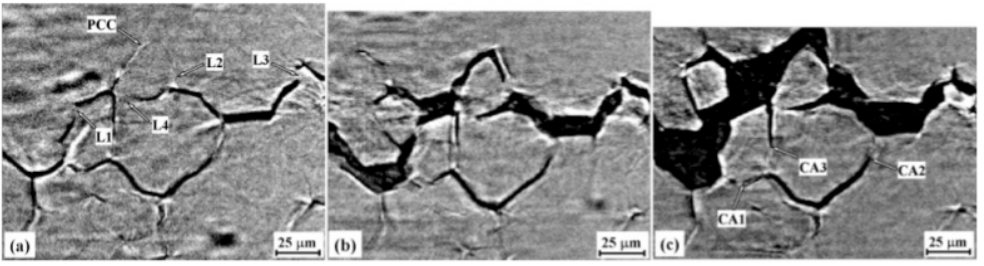

Figure 1: A sequence of images at the same location within a 3D volume of sensitised austenitic stainless steel undergoing intergranular stress corrosion cracking [10]. Several crack bridging ligaments develop and then fail as the crack opening increases.

Diffraction Contrast Tomography

This *non-destructive* synchrotron technique [14][15] enables full 3D characterization of the grain shape and crystal orientation in bulk samples with high resolution. A two-dimensional analogue is electron backscatter diffraction (EBSD), which provides a map of grain orientation on a suitably prepared surface. EBSD may provide a 3D map of microstructure, but this requires destructive serial sectioning [13]. The principal of the DCT technique is to observe the diffracted images of individual grains, simultaneously with their corresponding extinction images (i.e. dark shadows of the grains in the transmitted image). The sample is rotated in the path of the synchrotron X-ray beam, and the observed extinction and diffraction images are grouped into grain sets using criteria of shape, position and diffraction geometry. The crystallographic orientation of each grain is then

determined from the diffraction geometry, and the 3D shapes of the grains are obtained using the diffraction and extinction image projections. There are other related techniques for obtaining such 3D grain orientations [16][17]. However, DCT allows mapping of many hundreds of grains and is particularly suitable for crack nucleation studies, in which the sample size can be more than 10 grain diameters.

For example, the 3D mapping of the grain structure by DCT in a 300 μm diameter sensitised austenitic stainless steel sample was *followed* by in-situ 3D observations of SCC using CT [18]. Multiple crack nuclei developed, from which a dominant crack coalesced to propagate across the sample. The crack, observed by CT shortly before sample failure, is shown in Figure 2a, and is combined with the 3D map of the grains, obtained by DCT. Discontinuities or holes in the CT image of the crack due to crack bridging (e.g. Figure 1) were observed. An example is labelled as "Bridge 1" in Figure 2a. The crack path through a vertical plane at this location is superposed on a 2D map of the grain boundaries in Figure 2b. The grain boundaries are coloured according to their coincidence site lattice (CSL) designation. This defines the relative crystal orientation between adjacent grains. For example, annealing twins have the Σ3 CSL designation, and coherent Σ3 twins are resistant to sensitisation [19]. Bridge 1 coincides with a low angle grain boundary (i.e. Σ1), with a mis-orientation angle across the boundary of 9.4º±0.05º. The scanning electron microscopy image of the fracture surface in Figure 3 shows that failure was ductile at this location, confirming the development of a crack bridge that failed at high strain.

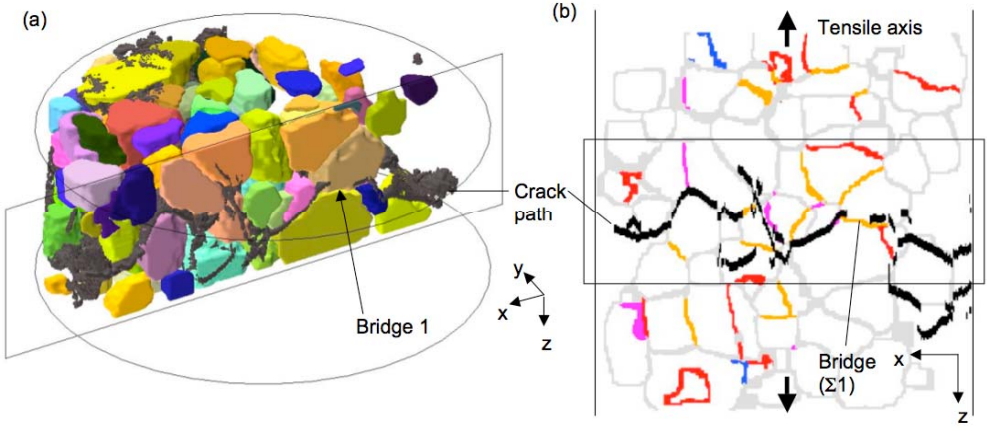

Figure 2: Combined DCT and CT data for an intergranular stress corrosion crack in sensitised austenitic stainless steel [18]: a) a 3D grain map, with grains coloured by orientation is sectioned through a crack bridge at Bridge 1 (the outline of the cylindrical sample is shown), b) a 2D map of grain boundaries in the plane of the section with the crack path shown with grain boundaries with low Σ CSL designations coloured as yellow (Σ1 or low angle boundary, red (Σ3), blue (Σ9) and purple (other boundaries Σ≤29).

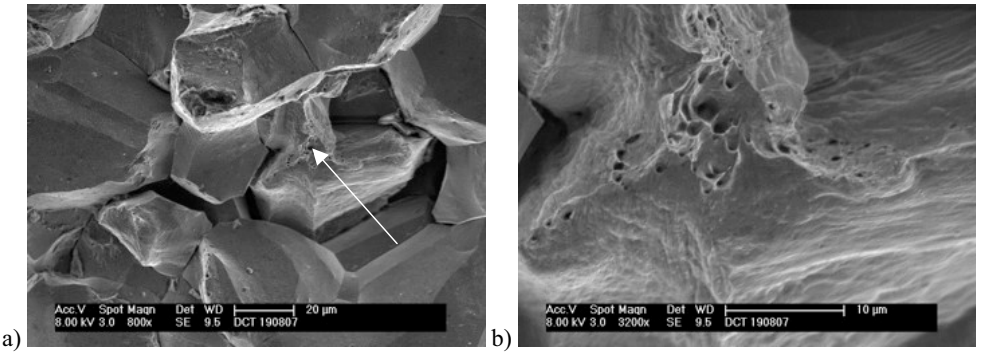

Figure 3: Scanning electron microscope image of the fracture surface at the location of Bridge 1 (see Figure 2) [18]. An arrow in marks Bridge 1 in a) and the higher magnification image of the ductile failure at this location is shown in b).

The CSL description of grain boundaries neglects the physical orientation of the grain boundary, which can significantly affect the grain boundary structure and its properties [20]. Although conventionally obtained by serial sectioning [13] or stereological methods [21], this can be obtained the DCT 3D mapping technique. The frequency distribution of grain boundary plane orientations in the bulk microstructure is shown in Figure 4, and is compared with the distribution of boundary orientations along the fracture surface. The boundary orientation is defined relative to each grain by fitting a flat plane between the two grains, thus two planes can be defined for each grain boundary. The Σ3 boundaries from coherent Σ3 annealing twins contribute strongly to a peak close to {111} due to their habit plane, but when these are excluded, there remains a preference of this plane in the other boundaries due to its low energy [22]. There is no preference for such boundaries on the fracture surface, however. This demonstrates a tendency for cracking along grain boundaries that not aligned close to low {hkl} index planes. Such boundaries have greater sensitisation resistance [19]. This observation is consistent with reports that grain boundary engineering to reduce the proportion of sensitised grain boundaries can improve intergranular SCC resistance [23].

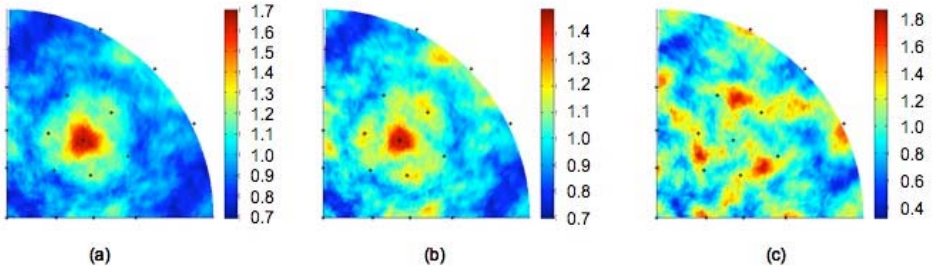

Figure 4: Stereographic projection pole figures showing the frequency distribution of grain boundary planes in the volume of grains in austenitic stainless steel [18]. The locations of {hkl} poles with low index are marked up to {221}; (a) All boundaries, (b) all boundaries excluding Σ3 twins, (c) only boundaries forming the fracture surface. The scale shows the proportion relative to the mean.

This example shows how the resistance of particular grain boundaries to intergranular stress corrosion cracking, and their role in crack bridge development, can be observed using the combined techniques of computed tomography and diffraction contrast tomography. Further work is in progress to characterise the detailed structure of the resistant boundaries. The data obtained are also

being used to develop 3D finite element crystal plasticity models (e.g. [13]) to describe the development of intergranular strains. The objective is to predict the observed crack nucleus behaviour relative to the microstructure, and thereby test the modelling of intergranular stress corrosion crack nucleation and growth. The same combined approach has recently been applied to fatigue crack nucleation in a Magnesium alloy, in which measurements of local crack growth rates and the crack orientation within the bulk of the sample have been obtained [24]. This allows direction observation of the transition between crystallographic, stage I, and non-crystallographic, stage II, propagation.

Surface Strain Mapping

Two-dimensional observations of the interaction between cracks and microstructure are also useful for short crack studies. Such studies do not need to be limited by the optical resolution relative to the crack opening displacements in order to observe cracks. Digital image correlation and ESPI (electronic speckle pattern interferometry) can provide high-resolution displacement measurements of surfaces, during deformation and cracking [25][26]. Differentiation of the crack opening displacements, measured at discrete intervals defined by a characteristic gauge length, can reveal cracks as regions of relatively high strain. This is shown schematically in Figure 5.

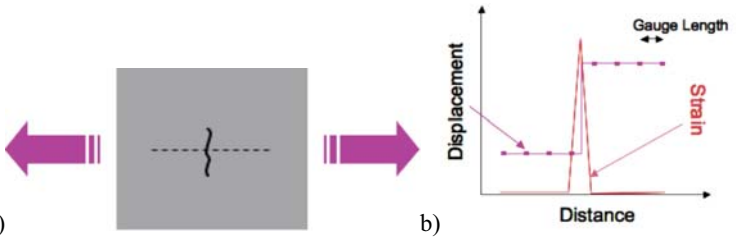

Figure 5: Illustration of crack visualisation by strain mapping; a) a crack under a tensile opening stress is shown, and the relative displacements are obtained at discrete locations with an interval of the measurement gauge length b) the opening displacement across the crack is differentiated to obtain a strain peak at the approximate location of the crack.

Such strain mapping is very sensitive to the small displacements from cracks, and can be used to observe and measure crack nucleation and growth rates. The derived strain maps resolve cracks with opening displacements that are non-resolvable by conventional techniques. The principles of crack imaging in brittle materials via opening displacements are well established [27]. Strain mapping techniques are quite readily applied due to advances in data processing capability and the performance of digital cameras. Two examples are given here, in which surface strain mapping has been used to study short crack nucleation and growth; in-situ observation of intergranular stress corrosion cracking in austenitic stainless steel, and cracking in nuclear graphite.

Crack Nucleation in Nuclear Graphite: Graphite is used as the moderator and also for structural components in first and second-generation carbon-dioxide gas-cooled nuclear fission reactors, such as the AGR reactors in the UK. It is also to be used in the next (third) generation of high temperature helium gas-cooled nuclear reactors. A well-founded, quantitative understanding of the behaviour of the microstructure under stress is important; a research aim is for the structural integrity of large graphite components of complex geometry to be predicted reliably from the assessment of relatively small test specimens. This requires validation of crack nucleation models (e.g. [28]) by direct observation of crack behaviour. This is experimentally difficult using conventional optical or Electron Microscopy techniques due to the complex porous microstructure of graphite, the small crack openings due to its low toughness, and the sparseness of crack nuclei.

High-resolution techniques are needed that allow observation of sufficiently representative surface area of the test specimen.

For example, ESPI (electronic speckle pattern interferometry) has been used to study crack nucleation in nuclear graphite [29]. ESPI is a full field strain mapping technique, and was applied to obtain in-situ, load resolved, strain fields from the surface of diametral compression specimens. The diametral compression [30] or Brazilian disc test is typically employed to determine the tensile strength of brittle materials. ESPI is an interferometric approach relying on a speckle pattern produced by laser illumination [31]. No specific surface preparation is required for a non-reflective surface, illuminated by a coherent (i.e. laser) light source that is split into a reference and an object beam. After reflecting from the sample surface these are recombined to form an interference image at the CCD.

In each test the sample was loaded progressively from a small pre-load without interruption until the sample failed or the maximum specified load was reached. Interference images of the sample were collected at intervals, and analysed to derive maps of the in-plane displacements. The ratios of the measured and calculated strains, obtained at each point from the displacement field gradient, define the strain ratio field. Strain localisation appears with high strain ratio as a magnification of the background horizontal elastic strain at that position. These 'strains' are not directly those present within the material, but are analogous to a very small strain gauge located on that point of the sample surface. As applied in this case, the strain gauge length is ~140 μm, with data obtained over an area of several millimetres square [29].

Analysis of strain fields was used to show the development of the distribution of localised deformation (i.e. regions of higher strain). This could be linked to the microstructure and damage processes that operated. Cracks were observed to nucleate at features such as regions of porosity (e.g. Figure 6). Failure was preceded by stable development of a critical crack nucleus, which propagated by micro-crack coalescence.

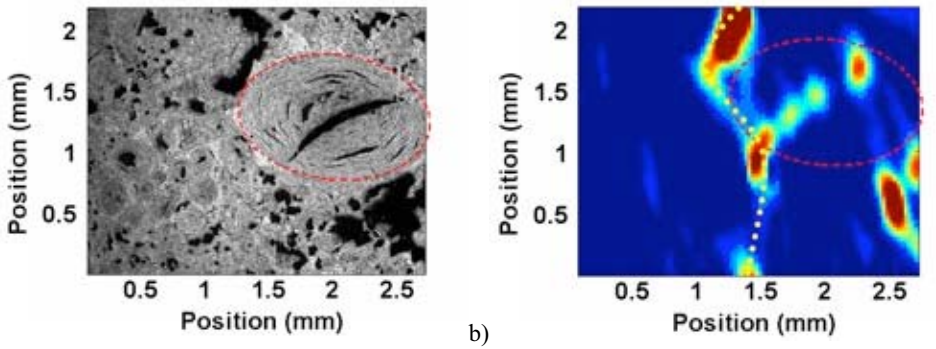

Figure 6: Strain localisation observed in nuclear graphite under load [29]. The tensile axis is horizontal; a) micrograph of part of the imaged area, with a characteristic filler particle outlined, b) map of horizontal strain for the same area. The fracture path is shown as a dotted line, and passes through a region of high strain associated with a cluster of pores.

These observations of the behaviour of small defects in nuclear graphite supported the general assumptions of graphite fracture models. They were also consistent with the view, for nuclear graphites, that the critical defect size and statistical descriptions of strength, such as Weibull modulus, could depend on test specimen geometry, stress state and size [28]. The crack nuclei were observed to be relatively sparse, compared to the microstructure scale. This was expected to affect

fracture behaviour in notched specimens and components, in which the highly stressed volume might be small relative to the microstructure scale.

Further work was therefore done to make in-situ observations of the distribution of crack nucleating defects in nuclear graphite, and their behaviour prior to unstable fracture, in a significantly larger area [32]. The low magnification necessary would normally make observation of cracks very difficult. For example, the crack opening displacement of a 1 mm deep semi-circular surface crack in tension at the typical failure stress of 25 MPa is less than 10 μm. However, such displacements can be observed using full-field strain mapping by digital image correlation (DIC) [26][33]. An image correlation system had been used to analyse high-resolution optical images of the surface of nuclear graphite specimens tested under four-point bend testing [32]. The field of view was approximately 100 x 100 mm, encompassing the entire tensile surface of each sample. Observations were made at frequent intervals up to almost immediately before failure. In comparison with the ESPI observations of disc specimens described previously, the effective strain gauge length in this case was approximately 0.6 mm.

An example of a surface strain map, obtained prior to failure, is shown in Figure 7. The final fracture path, determined from post-test examination of the broken sample, is shown as a dashed white line. It is coincident with two regions of high strain in the body of the observed region. Most tests showed the fracture path to be coincident with at least one such feature. However, some tests did not show any relation to such features, or none were observed. In some cases, the fracture path was connected to a high strain feature that was observed at the edge of the sample.

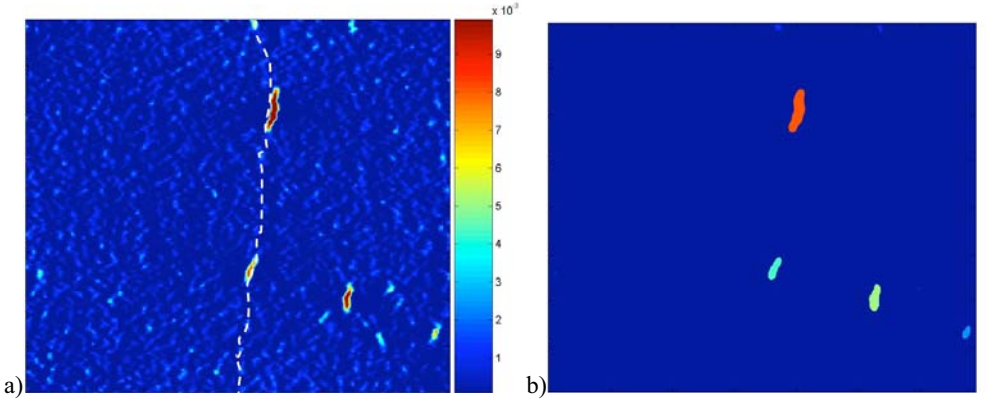

Figure 7: Identification of strain features, by in-situ observation [32]; a) a surface strain map (obtained immediately prior to failure) with the fracture path shown by the white dotted line; the area viewed is 100 x 100 mm, and corrections to the background strain have been made to account for specimen curvature), b) strain feature identification by threshold and segmentation, prior to measurement.

The surface length, and the opening strain ratio (i.e. the ratio of the maximum strain across the feature and the applied strain) could be measured throughout each test for every feature observed (Figure 8). Many features were observed to develop in length as the applied stress increased towards failure. The opening strain ratio tended to be initially constant, and then increased prior to failure. Assuming that the strain features are surface breaking cracks, the opening strain depends on the crack opening displacement and can be used to estimate the crack depth [32]. Lower strengths were observed to be associated with the deeper defects that develop prior to failure. The objective of these observations is to understand the relationship between initial defect size, loading geometry

and failure strength, and hence to link the statistics of failure to the initial defect size distribution. Work is now in progress to observe defect behaviour in a biaxial stress field.

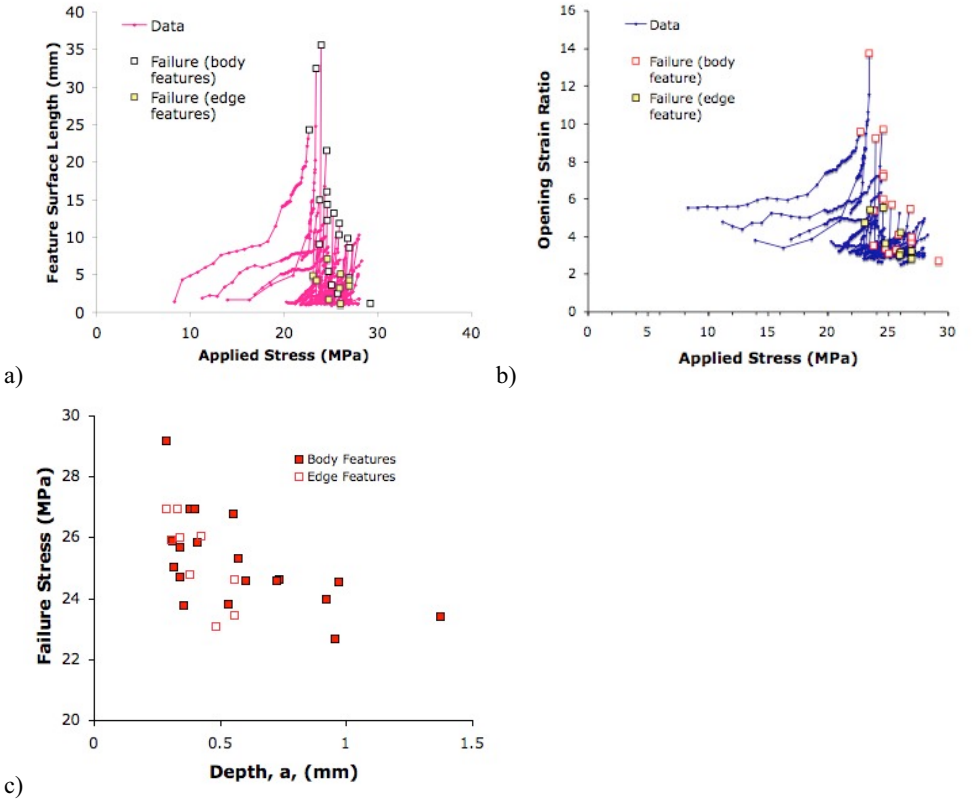

Figure 8: Observations of individual strain features in approximately 60 tests of nuclear graphite [32]; a) development of surface length with applied stress, b) development of opening strain ratio with applied stress, c) relationship between failure stress and crack depth (derived from the opening strain ratio of the strain feature). Features are identified as within the body of the sample, or in contact with the sample edge.

Intergranular stress corrosion cracking in austenitic stainless steel: There have been few studies of in-situ studies of stress corrosion in general (e.g. [34]), and very few for intergranular stress corrosion cracking, in particular [35][36] This is largely due to the difficulty in observing stress corrosion cracks whilst in the test environment. Image correlation techniques now enable such in-situ observations [37]. The effect of thermo-mechanical processing on short stress corrosion crack behaviour has also been studied using digital image correlation in thermally sensitised austenitic stainless steel. A solution annealed and thermo-mechanically processed steel were both tested under static load in the fully sensitised condition [38]. The observed regions were characterised prior to testing by EBSD. The thermo-mechanically processed microstructure has a more disrupted network of non-sensitised grain boundaries, which would tend to give greater resistance to intergranular stress corrosion cracking resistance. An example of the observation of crack development is shown in Figure 9, for the thermo-mechanically processed microstructure. In Figure 9a, the developed crack is revealed by after polishing and etching after the stress corrosion

test. Grain boundaries that are not cracked, but that are thermally sensitised, are also revealed by etching. The EBSD map for the same region is shown in Figure 9(b to d) with the development of the crack detected by image correlation analysis of successive optical micrographs. The crack is not at all visible in the original micrographs, but is revealed by image correlation. In this case, the total imaged area was approximately 1.5 mm x 2 mm (a selected area is shown in Figure 9) with an effective strain gauge length of 48 μm.

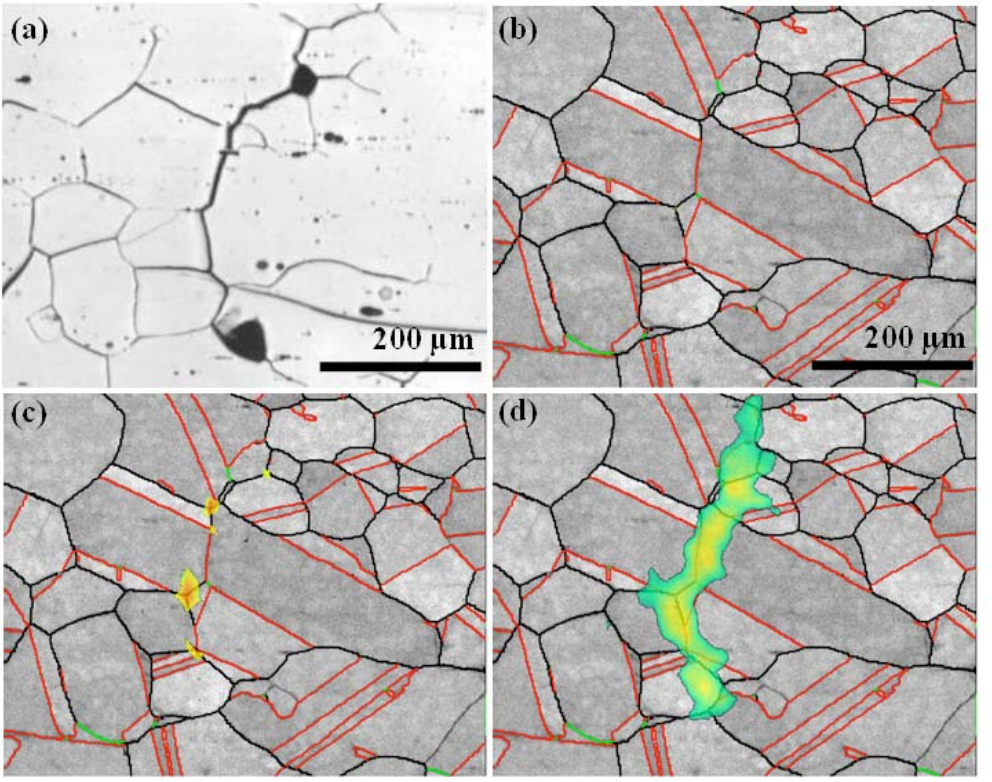

Figure 9: Correlation between observations of intergranular stress corrosion cracking in a thermo-mechanically processed microstructure of austenitic stainless steel [38], a) optical image of an intergranular crack after etching, b) the EBSD map of the same area of microstructure accompanied with superimposed strain map after 15 hours, c) the strain map obtained after 25 hours, d) strain map after 35 hours. The Σ3 twin boundaries are shown as red, and Σ9 boundaries as green.

The development of crack nuclei with time during the test can be measured, and was shown to vary significantly between microstructures (Figure 10) [38]. Nucleation was slowest in the thermo-mechanically processed microstructure. Observations such as Figure 9 show that cracks tend to initiate at grain boundaries without a low Σ CSL designation. The frequency of grain boundaries with high Σ CSL (i.e. Σ>29) designation along the crack path was also significantly lower than the average in the microstructure.

Work is currently in progress to relate crack nucleation behaviour to the network of susceptible grain boundaries, and to observe crack interactions with the microstructure as well as crack coalescence [33]. Combined with the 3D studies of microstructure and crack susceptibility (e.g

[18], the aim is to achieve greater inherent resistance to intergranular failure through control of the microstructure. Work is also in progress to obtain quantitative measurements of intergranular crack nucleation and growth in aggressive environments such as high temperature oxygenated water under dynamic loading, using a windowed autoclave system.

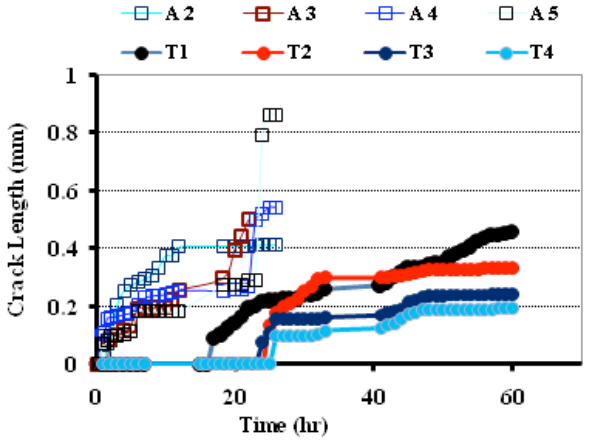

Figure 10: The development of individual crack nuclei with time in two different microstructures of sensitised austenitic stainless steel [38]. Cracks A2 to A5 are observed in a solution annealed microstructure, and cracks T1 to T4 are observed in a thermo-mechanically processed microstructure with a more disrupted network of corrosion susceptible grain boundaries.

Summary

New techniques for in-situ observations of crack growth behaviour include synchroton computed tomography, diffraction contrast tomography and surface strain mapping using electronic speckle pattern interferometry (ESPI) and digital image correlation. Examples of their application to stress corrosion cracking of stainless steels and brittle fracture of nuclear graphite have been presented. In each case, these techniques provide useful observations of the interaction between the crack and the microstructure.

Strain mapping techniques are not limited to two dimensions, and in suitable microstructures they can be applied to 3D data, such as computed tomography [40]. Such observations may provide in-situ quantitative measurements of relationships between crack driving force (i.e. crack opening displacement at the crack tip), microstructure and crack growth rate. Such research is necessary in order to develop and validate microstructure-based models for short crack behaviour.

Acknowledgements

The author is indebted to the significant number of co-researchers at the University of Manchester and collaborating researchers whose published work is illustrated in this paper. These include L. Babout, J-Y Buffiere (INSA-Lyon, France), J. Duff, D. Engelberg, A Hodgkins, G. Johnson, M. Joyce, A. King, H. Li, W. Ludwig (ESRF, Grenoble, France), S. Rahimi, P.J. Withers and P. Wood. The work presented here has been supported by organisations including EPSRC (Grant EP/C002946), Rolls Royce plc, British Energy Generation Ltd, Nexia Solutions and the University of Manchester. This support is gratefully acknowledged.

References

[1] K.J. Miller, Materials Science Perspective of Metal Fatigue Resistance, Mater. Sci. Technol. Vol. 9 (1993), p. 453

[2] R.W. Davidge and A.G. Evans, Strength of Ceramics, Materials Science and Engineering, Vol. 6 (1970), p. 281

[3] J. Dusza and M. Steen, Fractography and Fracture Mechanics Property Assessment of Advanced Structural Ceramics, International Materials Reviews, Vol. 44 (1999), p. 165

[4] A. Turnbull, Modelling of Environment Assisted Cracking, Corrosion Science, Vol. 34, (1993), p.921

[5] S.R. Stock, X-ray Microtomography of Materials. International Materials. Reviews. Vol. 44 (1999), p. 141

[6] T.J. Marrow, JY. Buffière, P.J. Withers, G. Johnson, D. Engelberg, High resolution X-ray Tomography of Short Fatigue Crack Nucleation in Austempered Ductile Cast Iron, Int. J. Fatigue Vol. 26 (2004), p. 717

[7] W. Ludwig, JY Buffière, S. Savelli and P. Cloetens, Study of the Interaction of a Short Fatigue Crack with Grain Boundaries in a Cast Al Alloy using X-Ray Microtomography. Acta. Materialia Vol. 51 (2003), p. 585

[8] E. Ferrie, JY. Buffière, W. Ludwig, A. Gravouil and L. Edwards, Fatigue Crack Propagation: In situ Visualization using X-ray Microtomography and 3D Simulation using the Extended Finite Element Method, Acta Materialia Vol. 54 (2006) ,p. 1111

[9] B.J. Connolly, D.A. Horner, S.J. Fox, A.J. Davenport, C. Padovani, S. Zhou, A. Turnbull, M. Preuss, N.P. Stevens, T.J. Marrow, JY. Buffière, E. Boller, A. Groso and M. Stampanoni, X-ray Microtomography Studies of Localised Corrosion and Transitions to Stress Corrosion Cracking, Mat Sci Tech. Vol. 22 (2006), p. 1076

[10] L. Babout, T.J. Marrow, D. Engleberg, and P.J. Withers, X-ray Microtomographic Observation of Intergranular Stress Corrosion Cracking in Sensitised Austenitic Stainless Steel, J. Mater Sci Tech. Vol. 22 (2006), p. 1068

[11] T.J. Marrow, L. Babout, A.P. Jivkov, P. Wood, D. Engelberg, N. Stevens, P.J. Withers, Three dimensional Observations and Modelling of Intergranular Stress Corrosion Cracking in Austenitic Stainless Steel, J Nuclear Materials Vol. 352 (2006), p. 62

[12] A.P. Jivkov and T.J. Marrow, Rates of Intergranular Environment Assisted Cracking in Three-dimensional Model Microstructures, Theoretical and Applied Fracture Mechanics Vol. 48 (2007), p. 187

[13] A.C. Lewis and A.B. Geltmacher, Image-based Modeling of the Response of Experimental 3D Microstructures to Mechanical Loading, Scripta Mater. Vol. 55 (2006), p. 81,

[14] W. Ludwig, S. Schmidt, E.M. Lauridsen and H.F. Poulsen, X-ray Diffraction Contrast Tomography: a Novel Technique for Three-dimensional Grain Mapping of Polycrystals. I. Direct Beam Case, J. Appl. Cryst. Vol. 41 (2008), p. 302

[15] G. Johnson, A. King, M.G. Honnicke, T.J. Marrow, W. Ludwig, X-ray Diffraction Contrast Tomography: a Novel Technique for Three-dimensional Grain Mapping of Polycrystals. II. The Combined Case, J. Appl. Cryst. Vol. 41 (2008), p. 310

[16] H.F. Poulsen, Three-Dimensional X-ray Diffraction Microscopy. Mapping Polycrystals and their Dynamics. Springer Tracts in Modern Physics. Berlin: Springer, (2004)

[17] B.C. Larson, W. Yang, G.E. Ice, J.D. Budai and J.Z. Tischler, Three-dimensional X-ray Structural Microscopy with Submicrometre Resolution, Nature (London) Vol. 415 (2002), p. 887

[18] A. King, G. Johnson, D. Engelberg, T.J. Marrow and W. Ludwig, Observations of Intergranular Stress Corrosion Cracking in a Grain Mapped Polycrystal, submitted to Science (2008)

[19] E.A. Trillo and L.E. Murr, Effects of Carbon Content, Deformation, and Interfacial Energetics on Carbide Precipitation and Corrosion Sensitization in 304 Stainless Steel, Acta Mater. Vol. 47 (1999), p. 235

[20] V. Randle, The Role of the Grain Boundary Plane in Cubic Polycrystals, (Overview) Acta Materialia Vol. 46 (1997), ,p. 1459

[21] V. Randle and H. Davies, A Comparison Between Three-dimensional and Two-dimensional Grain Boundary Plane Analysis, Ultramicroscopy, Vol. 90 (2002) p. 153

[22] M. Caul, J. Fiedler and V. Randle, Grain-boundary Plane Crystallography and Energy in Austenitic Steel, Scripta Met. Mat. Vol. 35 (1996), p. 831

[23] M. Shimada, H. Kokawa, Z.J. Wang, Y.S. Sato and I. Karibe, Optimization of Grain Boundary Character Distribution for Intergranular Corrosion Resistant 304 Stainless Steel by Twin-induced Grain Boundary Engineering. Acta Materialia Vol. 50 (2002), p. 2331

[24] T.J. Marrow, A. King, A. Khan, G. Johnson, JY. Buffière and W. Ludwig, Experiment Report MA423, Combined 3D Grain Mapping by Diffraction Contrast Tomography and in-situ Tomography Observations of Fatigue Crack Nucleation, European Synchrotron Radiation Facility, (2008)

[25] W.H. Peters and W.F. Ranson, Digital Imaging Techniques in Experimental Analysis, Optical Engineering, Vol. 21, (1982), p.427

[26] R.J. Sanford, Determining Fracture Parameters with Full-Field Optical Methods, Experimental Mechanics, Vol. 29, (1989), p. 241

[27] Z. Jia and S.P. Shah, Two-dimensional Electronic-speckle-pattern Interferometry and Concrete-fracture Processes, Experimental Mechanics, Vol. 34, (1994), p. 262

[28] T.D. Burchell, A Microstructurally Based Fracture Model for Polygranular Graphites. Carbon Vol. 34 (1996), p. 297

[29] M.R. Joyce, T.J. Marrow, P. Mummery, B.J. Marsden, Observation of Microstructure Deformation and Damage in Nuclear Graphite, Engineering Fracture Mechanics Vol. 75 (2008), p. 3633

[30] H. Awaji and S. Sato, Diametral Compressive Test Method. J Engineering Mater Technol. Vol. 101 (1979), p. 139

[31] L. Yang L and A. Ettemeyer, Strain Measurement by Three Dimensional Electronic Speckle Pattern Interferometry: Potentials, Limitations and Applications. J Optical Engineering Vol. 42 (2003), p. 1257

[32] H. Li, J. Duff and T.J. Marrow, PVP-2008 (Paper 61136), In-situ Observation of Crack Nucleation in Nuclear Graphite by Digital Image Correlation, Int. Conf. Press. Vessel. Piping, (2008)

[33] T.C. Chu, W.F. Ranson and M.A. Sutton, Applications of Digital-image-correlation Techniques to Experimental Mechanics, Experimental Mechanics, Vol. 25, (1985), p. 232

[34] R.N. Parkins and P.M. Singh, Stress Corrosion Crack Coalescence, Corrosion, Vol. 46 (1990), p. 485

[35] J. Nakano, Y. Miwa, T. Tsukada, S. Endo, and K. Hide, In situ SCC Observation on Neutron Irradiated Thermally-sensitized Austenitic Stainless Steel. Journal of Nuclear Materials, Vol. 367-370 (2007), p. 940

[36] M. Kamaya and T. Haruna, Crack Initiation Model for Sensitized 304 Stainless Steel in High Temperature Water, Corrosion Science, Vol. 48 (2006), p. 2442

[37] J. Duff and T.J. Marrow, PVP-2008 (Paper 61208), In-situ Observations of Intergranular Stress Corrosion Cracks, Int. Conf. Press. Vessel. Piping, (2008)

[38] S. Rahimi, D.L. Engelberg, J.A. Duff and T.J. Marrow, In-situ Observation of Intergranular Crack Nucleation in a Grain Boundary Controlled Austenitic Stainless Steel, submitted to J. Microscopy, (2008)

[39] N. Lenoir, M. Bornet, J. Desrues, P. Bésuelle and G. Viggiani, Volumetric digital image correlation applied to x-ray microtomography images from triaxial compression tests on argillaceous rock, Strain, Vol. 43, (2007), p. 193

[40] M. Kobayashi, H. Toda, Y. Kawai, T. Ohgaki, K. Uesugi, D.S. Wilkinson, T. Kobayashi, Y. Aoki and M. Nakazawa, High-density Three-dimensional mapping of Internal Strain by Tracking Microstructural Features, Acta Materialia, Vol. 56, (2008), p. 2167